FRONT MATTER

Title

- Amyloid-disrupted hippocampal spatial tuning and splitter cell activity leads to memory deficits in a spatial alternation task

Authors

Yimei Li,[1] Mary Ann Go,[1] Hualong Zhang,[1,2] Simon R Schultz[1*]

Affiliations

1. Centre for Neurotechnology and Department of Bioengineering, Imperial College London, United Kingdom
2. Department of Biomedical Engineering, University of Melbourne

Abstract

Alzheimer's disease (AD) is marked by progressive cognitive decline, yet the mechanisms underlying impaired memory encoding are not fully understood. To address this, we investigated hippocampal activity in 5xFAD mice performing a continuous spatial alternation task, combining head-fixed behavioural assessment with *in vivo* two-photon calcium imaging. 5xFAD mice exhibited deficits in alternation performance and task acquisition, which progressively worsened with age and were accompanied by behavioural hyperactivity and impaired speed modulation. Importantly, hippocampal CA1 neurons in 5xFAD mice showed impairments in spatial representation. Compared to non-5xFAD sibling controls, 5xFAD mice exhibited a lower proportion of place cells, reduced spatial information, and diminished trial-to-trial reliability. Moreover, reward location encoding was disrupted during goal-directed navigation. Despite these deficits, stable place cells retained relatively consistent spatial tuning across learning sessions. Finally, hippocampal trajectory-dependent activity (splitter cells) was significantly impaired in 5xFAD mice, with age-related declines in discriminability, reliability, and splitter extent. These impairments correlated with task performance and were more pronounced than behavioural deficits, suggesting that disrupted contextual encoding may precede and predict cognitive decline in AD. Together, our findings reveal early and progressive impairments in hippocampal spatial and contextual representations in 5xFAD mice, which contribute to behavioural deficits and provide insights into AD pathophysiology.

Teaser

Two-photon hippocampal imaging in behaving AD mice reveals impairments in spatial and contextual memory circuits contribute to cognitive deficits.

MAIN TEXT

Introduction

Alzheimer's disease (AD) is the most prevalent cause of dementia in older individuals, with a global prevalence particularly affecting those aged over 65 years (*1*). The amyloidogenic pathway generates amyloid-β (Aβ) and is implicated in other pathological features of AD, driving downstream pathophysiological signalling pathways that lead to neuronal death (*2-6*). Among cognitive impairments caused by the amyloidogenic pathway, spatial navigation deficits are particularly prominent, often detectable from the mild cognitive impairment stage (*7, 8*). Furthermore, it has been reported that more than 60% of AD patients suffer from spatial memory deficits and wandering behaviours (*9*). These deficits are closely linked to hippocampal dysfunction. The hippocampus, a critical component of the medial temporal lobe memory circuit, is essential for forming and retrieving spatial and episodic memory. In AD, hippocampal CA1 neuronal morphology, plasticity and neurogenesis are disrupted by Aβ and other pathological processes from early stages, as evidenced in both AD patients and mouse models (*10-12*).

Hippocampal place cells are essential for supporting spatial navigation and memory formation, yet they are degraded in AD. This degradation has been observed in various AD mouse models, including those with APP mutations and APP knock-in mice. For example, Tg2576 and hAPP mice exhibit disrupted hippocampal place fields and reduced spatial information, correlating with cognitive deficits (*13, 14*). In 3xTg AD mice, fewer hippocampal place cells exhibit phase-locking to theta and slow gamma rhythms prior to detectable Aβ accumulation (*15, 16*). 5xFAD mice show weakened synaptic efficacy and diminished sharp wave-ripples (SWRs) during place cell reactivation. Additionally, place cells in APP knock-in mice display impaired environmental remapping and disrupted context discrimination (*17*). Collectively, these findings suggest that dysfunctional hippocampal place cell firing contributes to instability in spatial representations and to AD-related memory deficits.

Early studies using tetrode recordings were limited in their capacity to record large neuronal populations, whereas calcium imaging combined with virtual reality-based behavioural paradigms, although scalable, lacks key sensory inputs that affect place cell activity (*18, 19*). One solution proposed for this is to use a floating, multimodal real-world maze which enables place-field mapping in head-fixed mice (*20*). Nevertheless, most studies have focused on relatively simple running tasks, despite evidence that tasks requiring mice to learn and adapt behavioural policies may be crucial for evaluating cognitive deficits in AD. Consequently, the specific alternations in place cell activity during learning and memory processes in AD models require further investigation.

Unlike place cells, which primarily encode spatial locations, splitter cells represent contextual information linked to memory and task demands. Splitter cells were first identified by Wood *et al.* and Frank *et al.*, who recorded hippocampal neuronal activity in rats performing a continuous T-maze alternation task (*21, 22*). They found that certain hippocampal neurons distinctly encoded different trajectories along a common path. This trajectory-dependent activity integrates computations of past experiences and future planning within a single neuron (*23*). However, the role of hippocampal splitters in AD-related cognitive dysfunction remains poorly understood. Previous studies suggest that synaptic changes induced by Aβ may trigger hippocampal learning and memory dysfunction

in AD mouse models (*24*). Moreover, rapid synaptic plasticity has been shown to play a key role in supporting hippocampal splitter cell activity (*25*). Therefore, we hypothesise that hippocampal splitting activity may degrade in AD mice. Given that hippocampal splitting activity integrate spatial and contextual coding during goal-directed, memory-guided navigation, they may serve as valuable targets for investigating the mechanisms of cognitive impairments in AD.

In this study, we investigated whether the degradation of hippocampal spatial and contextual representations at the neuronal level, including place cell and splitter cell activity, coincide with the onset of behavioural impairments in goal-directed learning in AD models. Focusing on the 5xFAD mouse model, which carries five familial AD mutations in the *APP* and *PSEN1* genes and rapidly develops severe amyloid pathology, we here introduce a novel behavioural paradigm. In this paradigm, head-fixed mice perform a continuous T-maze alternation task, the freely moving versions of which have previously been shown to be sensitive to hippocampal dysfunction (*26, 27*). By combining this task with two-photon calcium imaging, we recorded activity from large neuronal populations at the single-cell level, providing detailed insights into how AD affects hippocampal spatial coding and splitting function. Our findings confirm that alterations in spatially tuned hippocampal circuit activity in this mouse model of AD occur during, and affect performance in, a memory task in this AD mouse model. Importantly, we provide the first documentation of impaired hippocampal splitting activity in a spatial working memory task. These results highlight the potential for further examination of splitting activity as a target for investigating cognitive impairments in AD. This study advances our understanding of AD pathophysiology and may contribute to the development of more effective interventions.

Results

1. Head-fixed mice are able to acquire the continuous spatial alternation task in a floating real-world maze

We developed a novel behavioural paradigm to assess spatial memory in head-fixed mice, in which they performed a continuous spatial alternation task within a real-world, air-lifted maze setup. Our approach integrates the use of two-photon calcium imaging to capture the activity of populations of individual hippocampal neurons with high resolution during spatial navigation and memory tasks (Figure 1A, left). To motivate mice to navigate and learn the behavioural task, they were subjected to water restriction prior to the first day of training. In each trial, the mouse navigates from the location of the previous reward to the next reward location through a common pathway (Figure 1A, right). Mice are rewarded with 4 µl of liquid reward only when they choose the arm opposite to the one visited in the previous trial. The mice trajectories are recorded, and both correct and error trials are tracked across up to 10 days of training (Figure 1B). Behavioural performance is measured by the alternation percentage, which directly reflects learning and memory capabilities.

To validate the head-fixed alternation behavioural paradigm, we first trained young healthy mice (3–4 months old, N=10) in the task. Over the course of training, we observed a significant improvement in alternation percentage (Fig. 1B-D, $F_{(9, 81)} = 18.82$, $p < 0.001$, one-way RM ANOVA test). Head-fixed mice typically achieved a performance score of 70% by day 8, maintaining stable alternation performance through day 10. The total number of trials achieved per day (Fig. 1C, $F_{(9, 81)} = 13.11$, $p < 0.001$) was significantly increased, and trial latency was decreased (Fig. 1E, $F_{(9, 81)} = 6.50$, $p < 0.001$). These results indicate successful learning of the task in young healthy head-fixed mice. Furthermore, on error

trials, mice exhibited higher running speeds in the side arm compared to correct trials, while speed remained similar in the central arm (Fig.1F, see linearized trajectories in Fig. S1 A-C). This speed pattern suggests that the mice effectively recognized task-related movements, rather than engaging in random or gambled running behaviour. After successfully establishing the head-fixed behavioural paradigm, we used two-photon calcium imaging to record jGCaMP7s-expressing hippocampal CA1 pyramidal neurons in behaving head-fixed mice during the alternation task, extracting single-neuron calcium activity for further analysis (Fig. 1G-I, Fig. S1D).

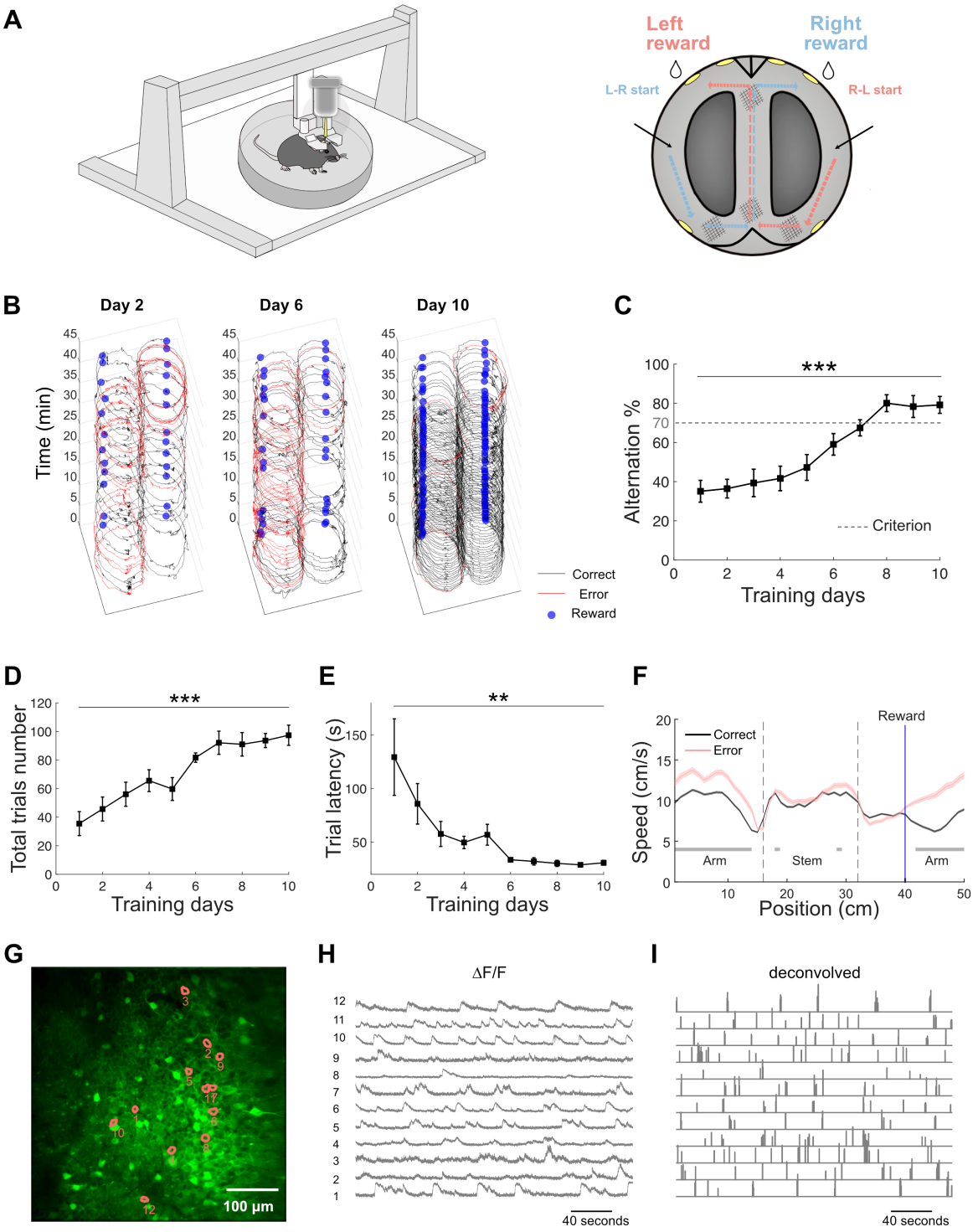

Figure 1. Head-fixed mice behavioural training and two-photon imaging in a continuous spatial alternation task

A. Left: Schematic showing a head-fixed mouse in the behavioural apparatus figure-8 maze. Right: Bird's eye view schematic of the air-lifted figure-8 maze. Correct trials: from left to right arm (blue), from right to left arm (red).

B. Temporal tracking of mouse position, differentiating between correct trials (black lines) and error trials (red lines) on the 2nd, 6th and 10th days of training, with reward locations demoted by blue dots.

C. Alternation percentage improved significantly over the training period. Horizontal dotted line indicates criterion (70%) for successful task acquisition.

D. The number of total trials per session in head-fixed mice grew significantly over training.

E. Trial latency (seconds) decreased significantly over training.

F. Animal speed during correct (black) and error (red) trials in the linearized trajectories calculated in 1 cm spatial bins. Vertical lines mark the start and end of the stem arm. Reward spout position is marked by a blue line. Grey shading shows spatial locations where the speed difference between correct and error trials is statistically significant. Linearized position (0 cm) starts are shown on the right of (A).

G. Representative field of view (FOV) in the hippocampal CA1 region, showing jGCaMP7s expression. 12 randomly selected ROIs overlaid in red.

H. Raw ΔF/F temporal traces from the neurons in (**G**).

I. Deconvolved activity traces from raw ΔF/F traces in (**H**), showing amplitude-event trains.

** and *** indicate the significance levels with the respective $P \leq 0.01$ and ≤ 0.001.

2. 5xFAD mice exhibited age-related behavioural deficits in the head-fixed spatial alternation task.

Previous studies have shown that intraneuronal Aβ42 is detectable in 5xFAD mice from 1.5 months of age, with extracellular Aβ deposition beginning around 2 months of age (*28, 29*). Aβ levels and amyloid burden increase sharply between 4 and 6 months (*28*), and the onset of learning and memory deficits emerge from 4 months (*30*). By 6 months of age, basal synaptic transmission and long-term potentiation (LTP) at hippocampal Schaffer collateral-CA1 synapses are reduced, alongside impaired contextual fear conditioning memory (*28, 31, 32*). Based on these findings, we defined a "young" AD group as mice younger than 4 months, and an "old" AD group as mice older than 7 months. After confirming that young non-AD mice could master the head-fixed alternation task within 10 days, we evaluated four groups of mice categorized by age and genotype (Fig. 2A): young (2–4 months) and old (7–12 months) mice, with genotypes defined as control (5xFAD−/−) and AD model (5xFAD+/−) mice (See Methods).

We observed that AD-related impairment in the head-fixed spatial alternation task in 5xFAD mice, was supported by a significant AD × training day interaction effect (Fig. 2B, $F_{(9,243)} = 2.53$, $p = 0.009$, two-way RM ANOVA test). All groups, except the old 5xFAD mice, exhibited significant improvement in the task perrformance over the training period. Young control mice demonstrated substantial improvement in alternation performance ($F_{(9,81)} = 18.82$, $p < 0.001$, one-way RM ANOVA test), as did old control mice ($F_{(9,45)} = 8.312$, $p < 0.001$) and young 5xFAD mice ($F_{(9,63)} = 4.63$, $p < 0.001$). In contrast, old 5xFAD mice did not show significant performance enhancement over time ($F_{(9,54)} = 1.38$, $p = 0.22$).

Furthermore, impaired alternation performance over training sessions was evident in old 5xFAD mice (AD × sessions interaction effect; $F_{(19, 209)} = 1.85$, $p = 0.02$, two-way RM ANOVA test), but not young 5xFAD ($F_{(19, 304)} = 1.21$, $p = 0.25$), when compared to their age-matched controls. Task acquisition was defined as achieving an alternation percentage of 70% or higher in three consecutive sessions or over two consecutive days. The task acquisition fraction further highlighted these differences, with old 5xFAD mice exhibiting the lowest proportion successfully acquiring the task during the training period (Fig. 2C). Within the 10-day training window, 8 out of 10 young control mice successfully met the task acquisition criteria. In contrast, 5 out of 8 young 5xFAD mice and 3 out of 6 old control mice reached the task acquisition criteria. The old 5xFAD group showed the most substantial impairment, with only 2 out of 7 mice achieving task acquisition.

Previous studies have reported hyperactive behaviours in both AD patients and mouse models of AD (*33, 34*). Consistent with this, we observed an age-related increase in the total number of trials completed (Fig. 2D, Age × AD effect, $F_{(1,270)} = 10.46$, $p = 0.0014$) and running speed (Fig. 2E, Age × AD effect, $F_{(1,270)} = 8.09$, $p = 0.0048$) over the training period in 5xFAD mice. This was accompanied by a reduction in trial latency (Fig. S2 A, B) during the task, indicating age-progressive behavioural hyperactivity in 5xFAD mice while performing the alternation task. Additionally, we observed age-related neuronal hyperactivity in the CA1 region (Fig. S2C, D). Furthermore, coherence between running speed and population-average hippocampal CA1 calcium activity was disrupted in old 5xFAD but not in young 5xFAD mice, relative to age-matched controls (Fig. 2F, G; OldCtrl *vs* OldAD, $p = 0.008$; YoungCtrl *vs* YoungAD, $p = 0.27$; two-way ANOVA test with Tukey-Kramer post hoc test.), indicating that 5xFAD showed age-related impaired speed modulation of CA1 neural activity during the head-fixed alternation task. Taken together, these findings demonstrate that 5xFAD mice exhibit cognitive and locomotor deficits in the head-fixed spatial alternation task.

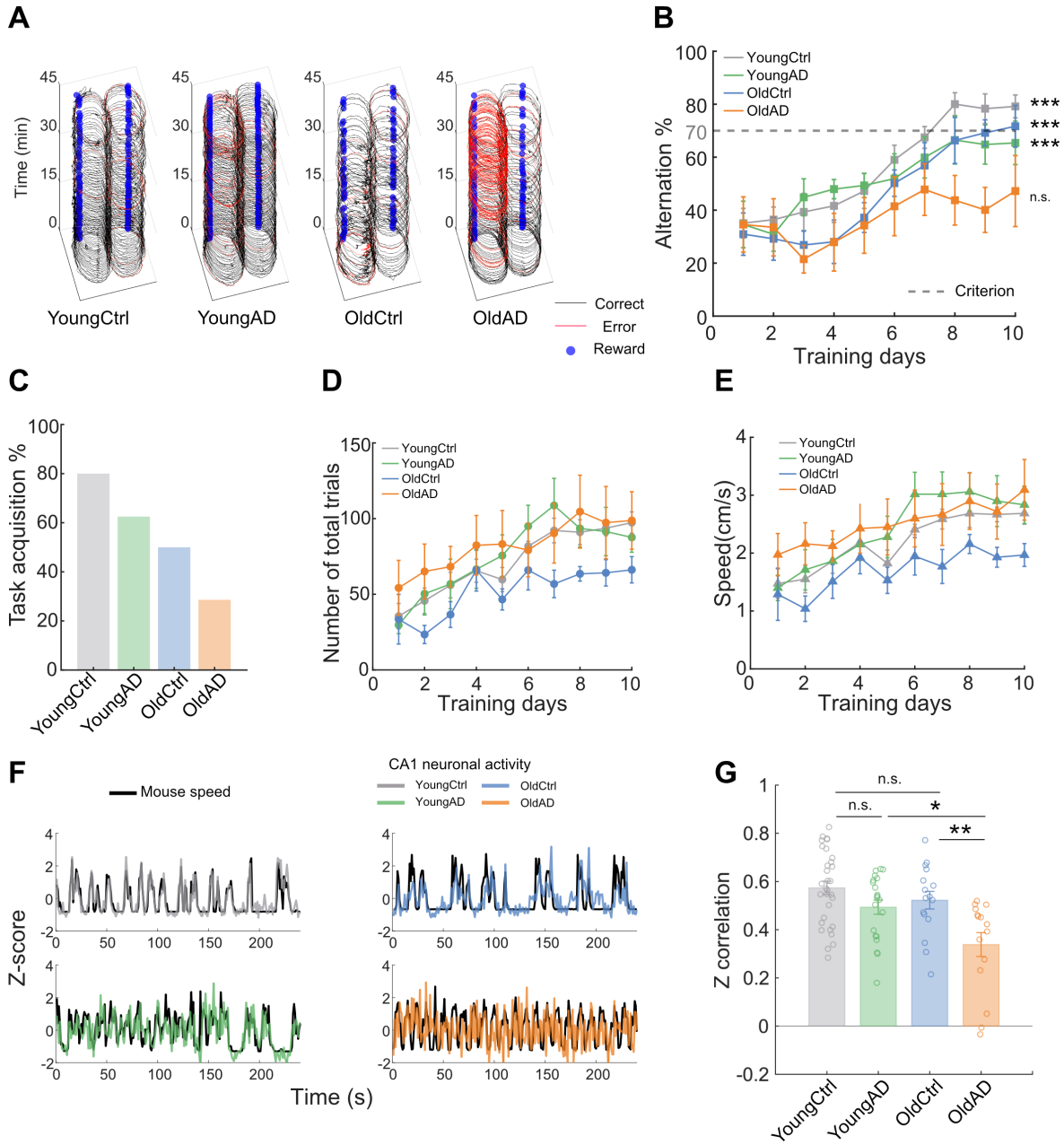

Figure 2. 5xFAD mice exhibited cognitive deficits and hyperactivity in head-fixed alternation task.

A. Representative temporal tracking of mouse position for each group on the final day of training, with correct trials are indicated by black lines, and error trials by red lines. Reward locations denoted by blue dots.

B. Percentage of correct alternations on each training day for all experimental groups. Young control (grey), Young 5xFAD (green), Old control (blue), Old 5xFAD (orange). Horizontal red dotted line indicates criterion (70%) for task acquisition. Two-way ANOVA test for group comparison. YoungCtrl N=10, YoungAD N=8, OldCtrl N=6, OldAD N=7.

C. Percentage of mice successfully acquiring the alternation task within 10 days for all groups. Task acquisition is defined as achieving an alternation percentage of 70% or higher in three consecutive sessions or over two consecutive days.

D. Total number of trials achieved per day for animals from all experimental groups.

E. Average speed (cm/s) on each training day from all experimental groups.

F. Representative time series data showing the Z-score of mouse locomotion speed (black) overlaid with the Z-score of mean neural calcium activity of the corresponding CA1 imaging FOV.

G. Correlation coefficient between animals' speed and population-averaged neural activity rate time series data for the corresponding imaging field of view. Data pooled from all imaging sessions in each animal group. See Table S1 for detailed statistics.

∗, ∗∗ and ∗∗∗ indicate the significance levels with the respective P values of ≤ 0.05, ≤0.01 and ≤ 0.001.

3. 5xFAD mice showed impaired spatial representations with unstable trial-to-trial spatial tuning

To determine whether hippocampal CA1 neurons in 5xFAD mice exhibit impaired spatial representations during the continuous spatial alternation task, we analysed hippocampal CA1 place cell activity across all trials. Calcium transient trains from each neuron were temporally aligned with the corresponding behavioural trajectory time points. The figure-8 maze was discretized into 1 cm-wide bins, forming a 32 × 32 grid, to construct spatial rate maps. For each bin, the spatial rate was calculated by dividing the sum of deconvolved calcium transient event amplitudes by the total time the mouse spent in that bin. Only running speeds greater than 8 mm/s were included in the spatial rate map calculation. A Gaussian kernel with a sigma value of [3, 3] bins was applied to smooth the spatial rate maps.

Although spatial tuning of neural activity was observed across all type of trials in both control and 5xFAD mice (Fig. 3A, B; See Fig. S3 A-B for place cells in the linearized trajectories across different type of trials), the proportion of place cells was significantly lower in 5xFAD mice compared to age matched controls (Fig. 3C,Young Ctrl 57±3% *vs* Young AD 45±4%, $p = 0.02$; Old Ctrl 41±3% *vs* Old AD 25±3%, $p = 0.02$; two-way ANOVA test with Tukey-Kramer post hoc test). Additionally, 5xFAD mice exhibited significant age-related reductions in spatial information compared to age matched controls (Fig. 3D, Young Ctrl 3.83±0.03 *vs* Young AD 3.32±0.03, $p < 0.001$; Old Ctrl 3.13±0.05 *vs* Old AD 2.79±0.04, $p < 0.001$; Scheirer-Ray-Hare test with the Dunn-Sidak post hoc test).

To assess the stability of spatial tuning across trials in CA1 neurons of 5xFAD mice within each imaging session, we analyzed the fraction of trials in which place cells remained active during the alternation task training. This was measured as the number of trials in which place cells remained active, divided by the total number of trials within same type of trajectory. 5xFAD mice showed an age-progressive reduction in th proportion of trials exhibiting spatially tuned activity (Fig. 3E; AD×Age interaction effect: $H_{(1,28516)} = 3.97$, $p = 0.046$, Young Ctrl *vs* Young AD, $p < 0.001$; Old Ctrl *vs* Old AD, $p < 0.001$; Scheirer-Ray-Hare test with the Dunn-Sidak post hoc test), suggesting a decline in the consistency of place cell activity over trials. The trial-to-trial spatial correlations show stabilization of the spatial coding within the imaging session. To further examine this, we calculated spearman correlation coefficients between spatially binned activity on adjacent trials within the same imaging session. Our results revealed that CA1 place cells in 5xFAD mice exhibited a progressive age-related decline in trial-to-trial spatial stability (Fig. 3F, G. AD×Age interaction effect: $H_{(1, 28469)} = 34.79$, $p < 0.001$; Young Ctrl *vs* Young AD, $p < 0.001$; Old Ctrl *vs* Old AD, $p = 0.008$). Notably, similar deficits were observed in both correct and error trials (Fig. S3 C-D). These impairments, characterised by a lower proportion of active trials and reduced spatial stability, emerged at a young age in 5xFAD mice and were consistent

with a decreased proportion of place cells and impaired spatial information (Fig. 3C-D). However, behavioural performance during alternation task imaging sessions was relatively preserved in young 5xFAD mice, with no significant deficits compared to age-matched controls (Fig. S3 E, p = 0.45), whereas old 5xFAD mice exhibited a significant reduction (p = 0.04), consistent with behavioural training results across days (Fig. 2B). Overall, these findings suggest that place cell deficits in 5xFAD mice are pronounced from an early age, while behavioural impairments become more evident with age. This indicates that disruptions in spatial coding may occur predict detectable cognitive deficits in alternation task performance.

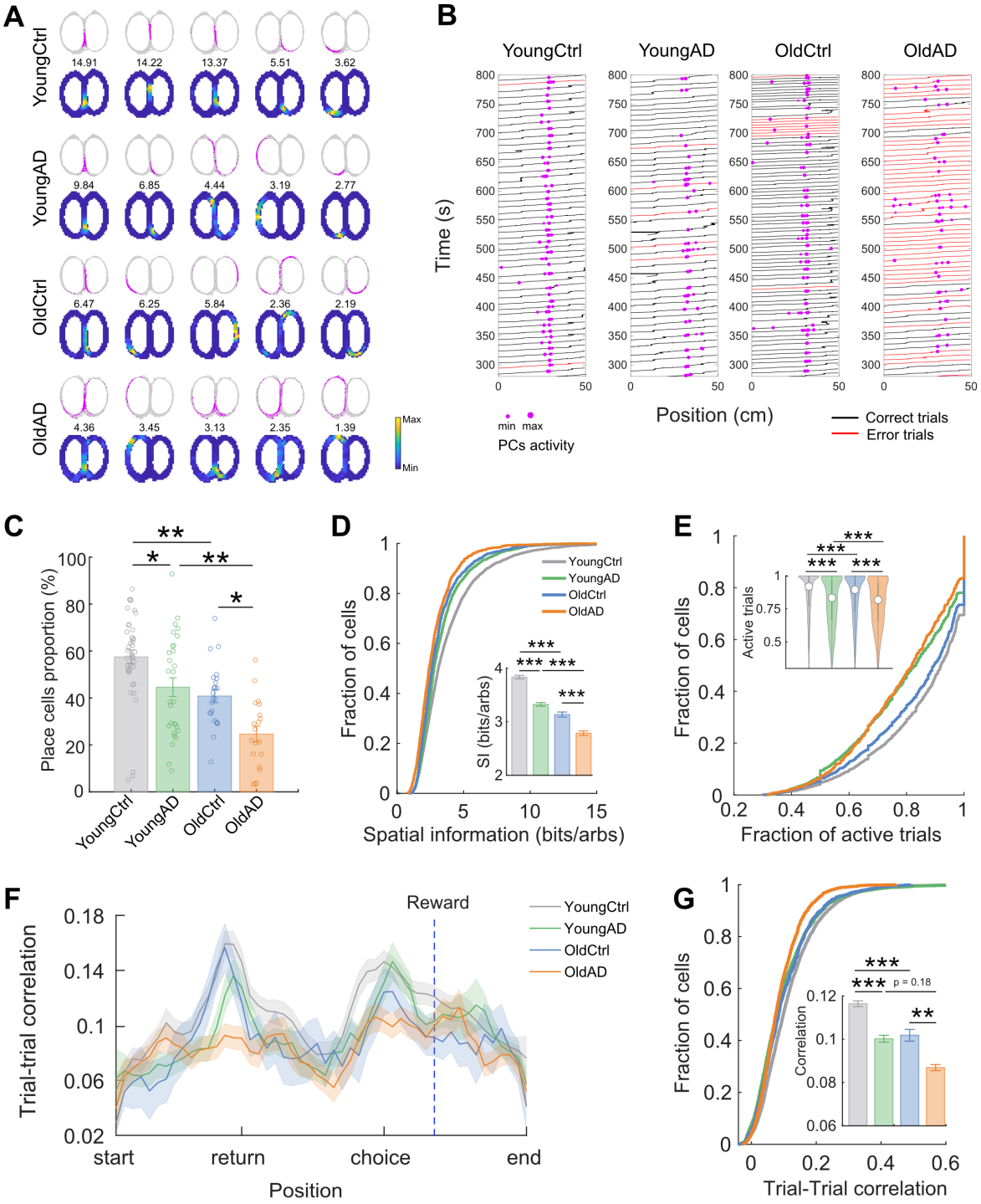

Figure 3. 5xFAD mice show impaired spatial representations with reduced trial-to-trial spatial tuning stability

A. Five representative CA1 place cells in young control, young 5xFAD, old control and old 5xFAD, respectively. Raster plots (upper panels, calcium activity in magenta dots and mouse trajectory in grey lines) and normalized neural activity rate map (lower panels); Skagg's spatial information (bits/arb) is indicated for each representative place cell.
B. Temporal tracking of mouse linearized position, showing typical examples of place cell activity throughout trajectories during each trial. Black line: position on correct trials, Red line: position on error trials, Magenta dots: place cell activity.
C. The percentage of neurons meeting "place cell" criteria was reduced in 5xFAD mice.
D. Cumulative distribution of spatial information (Skaggs information, bits/arb) for each mouse group, with inset bar plot showing mean ± s.e.m..
E. Cumulative distribution with inset violin plots show the proportion of trials in which place cells were active, as a distribution across all imaging sessions. Violin plots show median, minimum and maximum values.
F. Trial-to-trial correlation (mean adjacent trial-to-trial Spearman correlation of spatially binned activity) of CA1 spatial tuning across position, for each mouse group. Shading represents mean ± s.e.m. across cells. Blue dotted line showed the position of the reward.
G. Cumulative distribution with inset bar plots illustrate the mean trial-to-trial stability of place cells (average of trial-trial correlation across all spatial bins in each cells).
$*$, $**$ and $***$ indicate the significance levels with the respective p values of < 0.05, < 0.01 and < 0.001. See Table S1 for detailed statistics.

4. Preserved session-to-session spatial stability in 5xFAD mice

The long-term stability of place cells is believed to support the hippocampal contribution to long-term memory (*35, 36*). We next examined whether the session-to-session spatial tuned activity across alternation behavioural training was degraded in 5xFAD mice. To assess the stability of place cells across the training process, we imaged the same FOVs across 3 training stages: early (day 6), middle (day 8) and final (after day 10) (Fig. 4A). By registering images from the same FOV across these stages, we were able to track the same population of neurons. Next, we identified neurons classified as place cells during each imaging stage. After sorting the peak activity of each place field at each stage, we observed that some place cells maintain stable spatial tuning across sessions (Fig. 4B). Therefore, we defined stable place cells as those that exhibited significant spatially tuned activity across all three training stages (Fig. 4C).

First, we observed that some place cells exhibited persistent and stable place field firing across all imaging stages, even in old 5xFAD mice (Fig. 4D). Although the proportion of stable place cells was lower in 5xFAD mice compared to age-matched controls, the difference was not statistically significant. However, a significant reduction in the proportion of stable place cells relative to the total number of place cells was observed at all imaging stages in aged 5xFAD mice compared to young control mice (Fig. 4E; early stage: $p = 0.01$; middle stage: $p = 0.01$; final stage: $p = 0.005$; Two-way ANOVA test with Tukey-Kramer post hoc test). This finding is further supported by the reduced proportion of stable place cells relative to all recorded cells (YoungCtrl *vs.* OldAD, $p = 0.006$). Furthermore, among the four groups, only old 5xFAD mice displayed changes in place field size across imaging stages (Fig. S4, $\chi^2 = 10.06$, $p = 0.007$, Kruskal-Wallis test).

To further examine whether the spatial stability of those stable place cells was altered over days in 5xFAD mice, we quantified the session-to-session spatial correlation of place cells across training stages. Interestingly, both young and aged 5xFAD mice exhibited session-to-session correlations comparable to those of control mice (Fig. 4G, Young Ctrl *vs* Young AD: p = 0.18; Old Ctrl vs Old AD: p = 0.98; Young Ctrl vs Old AD: p = 1; Scheirer-Ray-Hare test with the Dunn-Sidak post hoc test). Moreover, persistent place cells in 5xFAD mice did not exhibit significant shifts in the peak activity location of place fields across sessions. (Fig. 4H, AD effect: H(1, 1304) = 1.7; P = 0.2). These findings suggest that while place field size of stable place cells fluctuates in old 5xFAD mice, peak activity locations within place fields and spatial tuning maps remain relatively stable during the alternation task. This indicates that 5xFAD mice can still sustain a subset of place cells for stable spatial representations in a familiar environment. Notably, these results contrast with the impaired trial-to-trial stability observed in 5xFAD mice (Fig. 3F-G), suggesting that while long-term spatial representations remain relatively preserved, the short-term reactivation of spatial maps during the alternation task is more vulnerable to disruption.

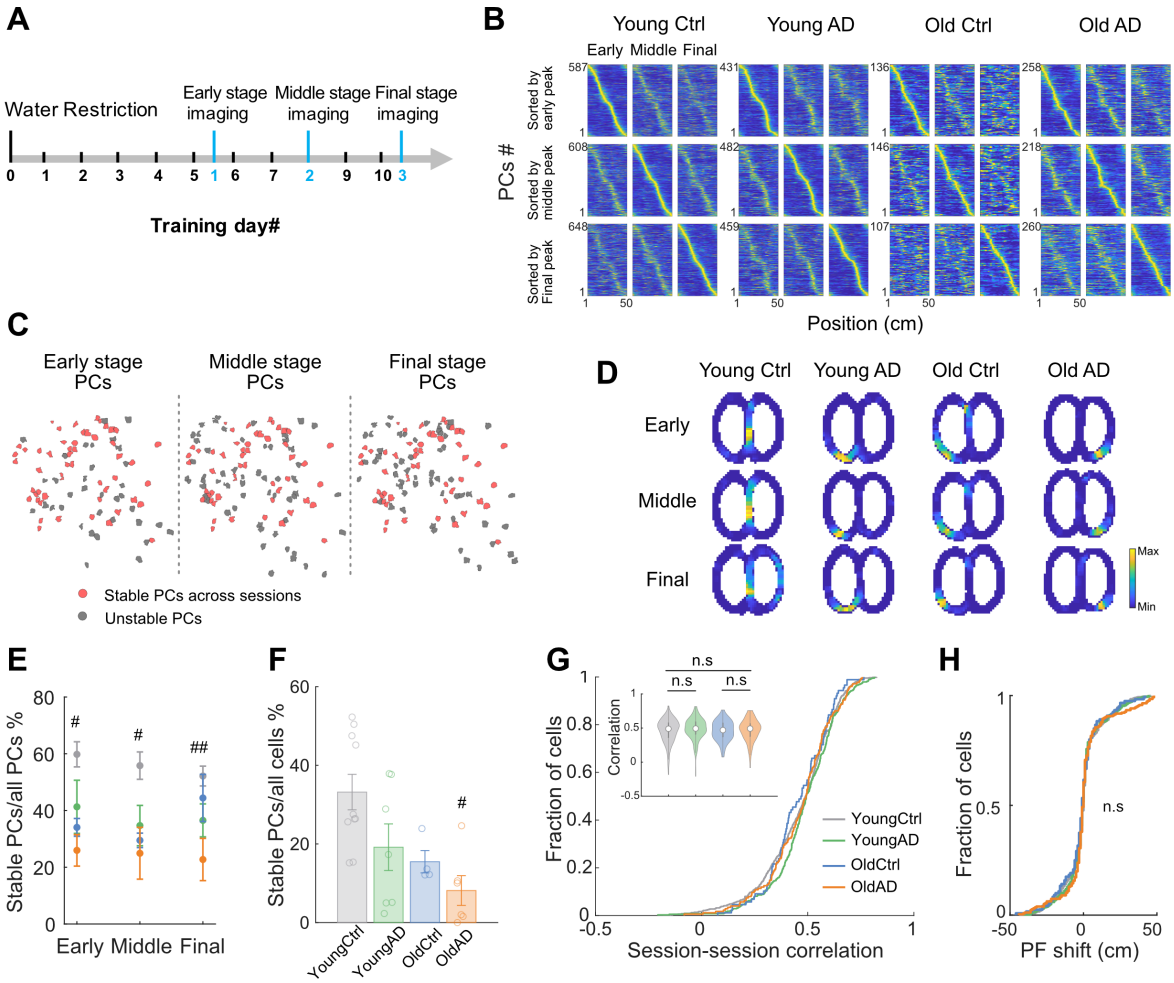

Figure 4. Stable place cells across sessions in 5xFAD mice

A. Timeline of the imaging sessions across the training task, including early-stage imaging (around the 6th training day), middle stage imaging (around the 8th training day), and final stage imaging (after the 10th training day).

B. Distribution of place fields along a linear trajectory, sorted by place cells at each experimental stage.

C. Place cells from an example FOV during the early, middle and final stage, with red contours indicating place cells that maintained spatial tuning activity across early, middle, and final stages (Stable place cells).

D. Representative spatial maps for stable place cells throughout the training phase in both control and 5xFAD mice.

E. The proportion of place cells that persisted across all stages (stable place cells) to the number of all place cells (PCs) identified at each individual stage. # indicates a statistically significant difference between old 5xFAD and young control mice.

F. Proportion of stable place cells to the number of all tracked cells across sessions.

G. Cumulative plots with inset violin plots show the session-to-session spatial correlation coefficients of stable place cells in all mouse groups. 5xFAD mice did not show reduced spatial correlations. Scheirer-Ray-Hare Test with Dunn's post hoc test.

H. Place field shift of stable place cells from early stage to final stage in control and 5xFAD mice.

n.s. represents not significant. # and # # indicate the significance levels with the p values of < 0.05 and < 0.01. See Table S1 for detailed statistical results.

5. 5xFAD place cells exhibit impaired spatial encoding of the reward location

Accurate encoding of reward locations is essential for successful goal-directed navigation. Given the reward-driven nature of our alternation task, we examined how hippocampal place cells responded to reward locations during both correct and error trials. The reward arm was defined as the segment of the maze beyond the choice point (Fig. 5A). Trials were categorized by turn direction: correct left turns (RL) overlapped with error left turns (LL) shared the same reward location, as did correct right turns (LR) and error right turns (RR). Mice were not rewarded during error trials (RR and LL).

To examine spatial coding along reward arms, we analysed the activity of place cells which had place fields along the reward arm. Since correct and error trajectories overlapped at the reward location, these place cells exhibited spatial tuning for both trial types (Fig. 5B). We then compared their spatial tuning activity during rewarded correct trials (Fig. 5C) and unrewarded error trials (Fig. 5D). Place cells along the reward arm showed increased activity near the reward spout position in both trial types, with a decline after the reward spout. However, in 5xFAD mice, the peak spatial tuned activity at the reward spout was significant reduced in correct trials (Fig. 5C AD effect: $H_{(1,9127)}= 77.45$, $p < 0.001$; Young Ctrl *vs* Young AD: $p < 0.001$; Old Ctrl vs Old AD: $p < 0.001$; Scheirer-Ray-Hare test with the Dunn-Sidak post hoc test), with a progressive decline observed with age (AD×Age effect: $H_{(1,9127)}= 17.05$, $p < 0.001$). In error trials, although spatial tuned activity was also significantly reduced (Fig. 5D. AD effect: $H_{(1,8474)}= 57.74$, $p < 0.001$; Young Ctrl *vs* Young AD: $p < 0.001$; Old Ctrl vs Old AD: $p =0.019$), this reduction did not exhibit a clear age-related pattern (AD×Age effect: $H_{(1,8474)}= 2.23$, $p = 0.16$).

We next assessed whether hippocampal neurons in 5xFAD mice are able to accurately encode the reward spout location during rewarded trials. In old, but not young, 5xFAD mice, the peak neuronal activity was significantly displaced from the reward spout, shifting towards the post-reward arm. (Fig. S5, Young Ctrl *vs* Young AD: $p = 0.44$; Old Ctrl vs Old AD: $p < 0.001$). To further evaluate the consistency of spatial encoding, we examined the spatial correlation of place cells activity between correct and error trials along reward arms. 5xFAD mice exhibited an age-dependent reduction in spatial correlation, suggesting a diminished ability to consistently encode reward positions across trial types (Fig. 5F, G;

AD×Age effect: $H_{(1,7332)} = 18.12$, $P < 0.001$; YoungCtrl *vs* YoungAD: $p < 0.001$; OldCtrl *vs* Old AD: $p = 0.0088$). However, this reduction was not observed in place cells that have place fields in the return arms (Fig. S6A-C), indicating these deficits are specific to the reward arm. These findings suggest that the impaired reward location encoding in 5xFAD mice results from both deficits in spatial representation of the reward and disruptions in reward-related contextual processing, with impairments emerging as early as the young age group.

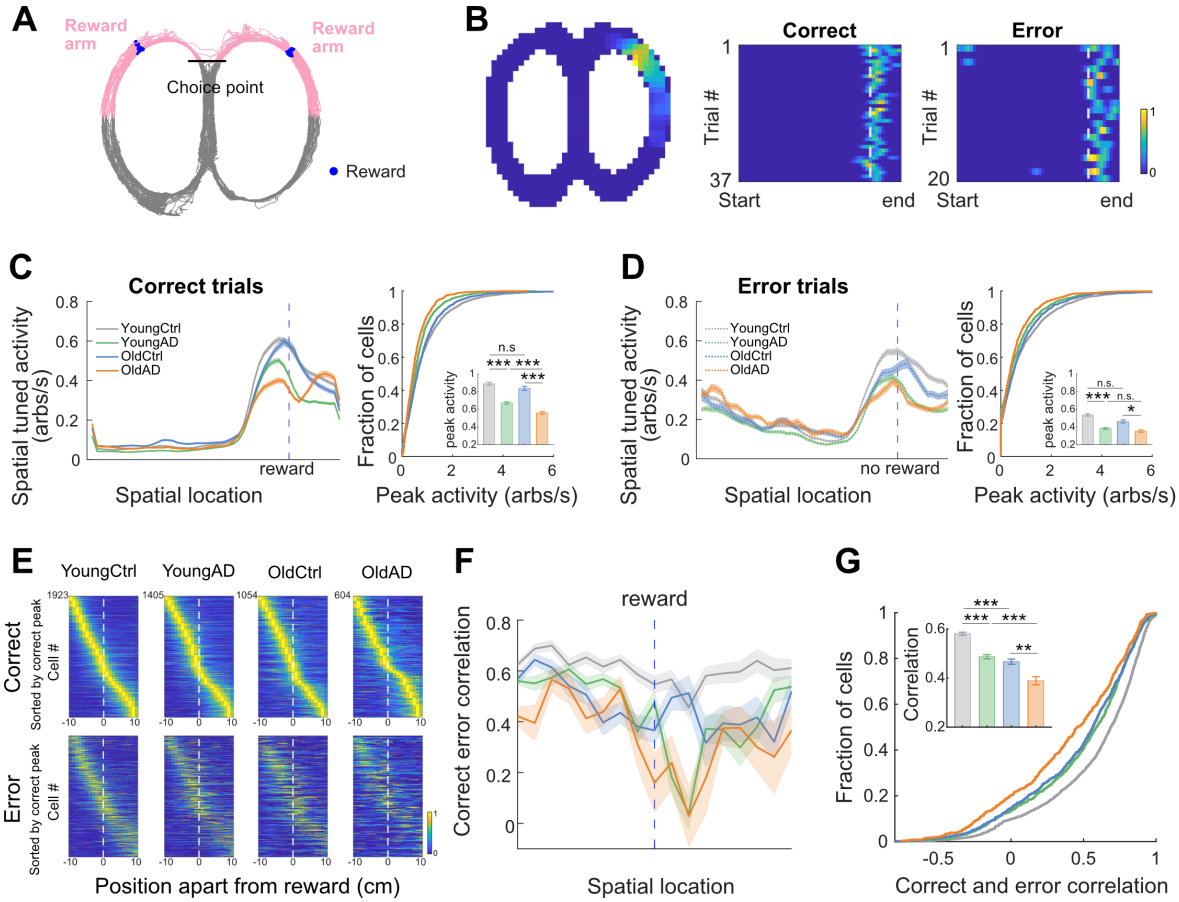

Figure 5: 5xFAD place cells show reduced activity in the reward arm

A. Typical mouse trajectory in a continuous alternation task session. Choice-reward arm (pink), reward location (blue), and other arms (grey) are indicated.

B. Example of a place cell spatial activity map which has place fields along the reward arm (Left). Reward spatial tuned activity on every correct trial (middle) and error trial (right). White dotted lines show reward position.

C. Left: spatial activity profile of reward-arm place cells during correct trials (data was pooled from all reward place cells in all imaging sessions). Shading represents mean ± s.e.m. across cells. Blue dotted lines show reward position. Right: cumulative plots with inset bar plots show the peak spatial tuned activity at the reward spout location. For better clarity, values on the X-axis greater than 6 are not shown in the figure.

D. As as C, but for error trials.

E. Normalized peak place cell activity along reward arm position. Top: correct trials, Bottom: error trials. Sorted by peak activity during correct trials. White dotted lines show reward position.

F. Spearman correlation coefficients of reward-arm place cell activity (all reward place cells pooled) between correct and error trials along the spatial location. Shading represents mean ± s.e.m. across cells.

G. Cumulative plots with inset bar plots show the spatial correlation of reward-arm place cell activity between correct and error trials (from (F)). Bar plots show data as mean ± s.e.m..

∗, ∗∗ and ∗∗∗ indicate significance levels with respective p values of < 0.05, < 0.01 and < 0.0001. See Table S1 for detailed statistical results.

6. Hippocampal CA1 neural splitting activity degraded in 5xFAD mice

A splitter cell is a type of neuron whose tuning of activity on a common path (here, the stem arm) varies according to the trajectory chosen by the animal. Splitter cells are thought to represent contextual information linked to memory and task demands, reflecting an internally organized process that adapts to varying cognitive and behavioural contexts (*37, 38*). To identify splitter cells, we examined neurons with a place field spanning at least five spatial bins along the stem arm that exhibited trajectory-dependent activity during correct trials (see methods). Our analysis revealed representative hippocampal CA1 cells showing significant splitting activity for each turn direction across all groups (Fig. 6A, B), as well as stem place cells that did not display significant splitting activity (Fig. S7 A-E). To our knowledge, this study presents the first documentation of hippocampal splitter cells in a mouse model of AD.

To investigate how hippocampal splitter cells were altered in 5xFAD mice, we quantified the proportion of splitter cells, the ratio of splitter cells to stem place cells, and the overall proportion of stem place cells. A significant positive correlation was observed between alternation performance and the ratio of splitter cells (Fig. 6C, $R = 0.31$, $p < 0.001$, Pearson correlation), with a stronger correlation found for the ratio of splitter cells to stem place cells (Fig. 6D, $R = 0.55$, $p < 0.001$). In contrast, the proportion of stem place cells alone did not correlate with performance (Fig. 6E, $R = -0.04$, $p= 0.67$). This suggests that impaired behavioural performance is associated with reduced splitter cells specifically, rather than general stem place cell representation. Moreover, we observed a significant reduction in the proportion of splitter cells in old 5xFAD mice compared to young controls (Fig. S7. F, $p = 0.008$). To further assess splitting activity at the population level, we trained a linear discriminant analysis (LDA) decoder to classify future turn direction at each spatial bin along the stem arm. The decoder's classification accuracy also positively correlated with alternation performance (Fig. 6F, $R = 0.25$, $p = 0.0088$), further reinforcing the association between altered splitting activity and cognitive dysfunction.

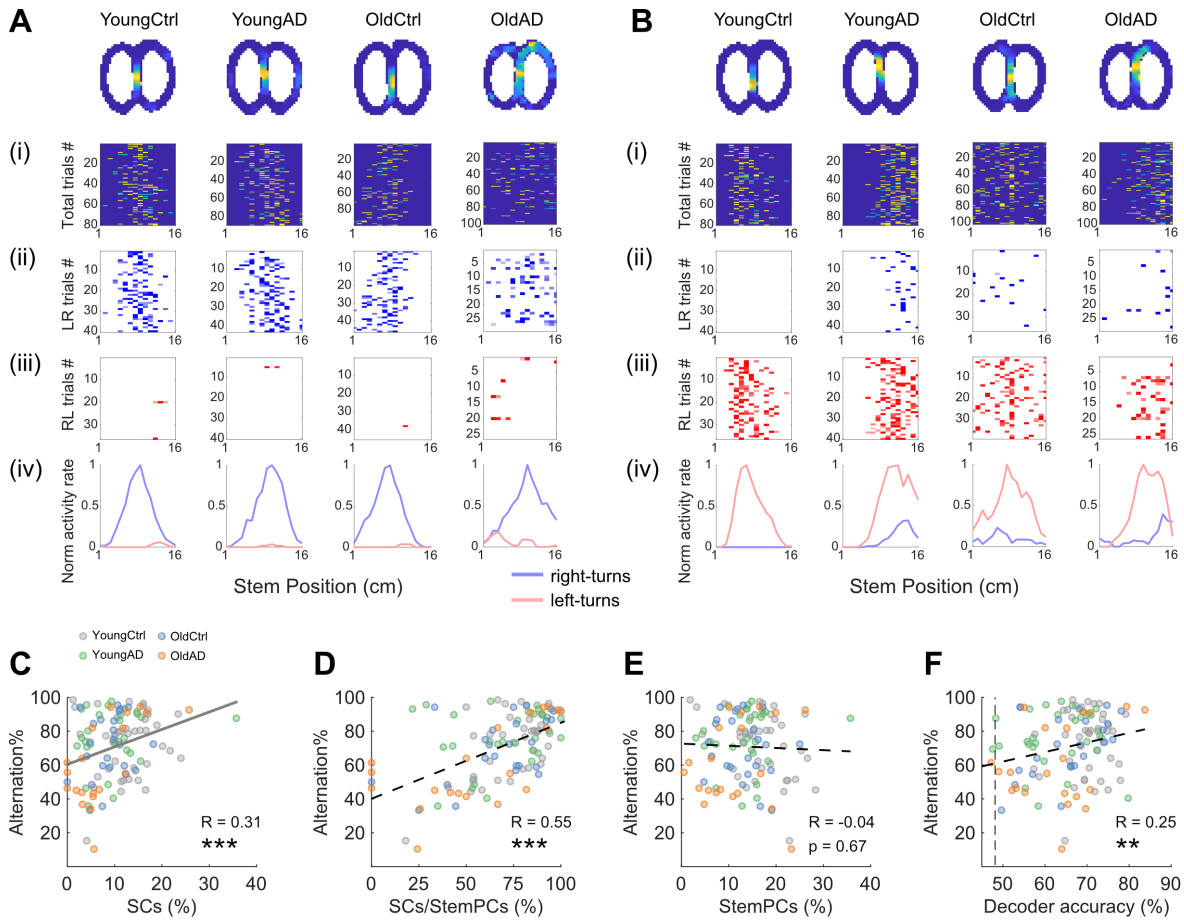

Figure 6. Hippocampal splitter cells are observed in 5xFAD mice

A. Four representative stem place cells, one for each group. Each column, top to bottom: (i) Normalized calcium activity 2D occupancy map for the figure-8 maze for one imaging session; (ii) Neuronal calcium activity raster along the stem for all trials in the figure-8 maze, linearized profile from the same imaging session; (iii) Neuronal calcium activity raster along the stem for all left-right trials (blue) from same imaging session; (iv) Neuronal calcium activity raster along the stem for all left-right trials (red) from same imaging session; (iv) Normalised calcium tuning curves for each turn direction. blue: left-right turn, red: right-left turn.

B. As for **A** but for representative splitter cells dependent on right-left turns.

C. Ratio of splitter cells to all cells versus behavioural alternation performance.

D. Ratio of splitter cells to stem place cells versus behavioural alternation performance.

E. Ratio of stem place cells to all cells versus behavioural alternation performance.

F. Mean classification decoder accuracy for all cells versus behavioural alternation performance for each imaging session.

Data pooled across all imaging sessions. Pearson correlation. $*$, $**$ and $***$ indicate significance levels with respective p values of < 0.05, < 0.01 and < 0.001.

To further investigate the impairment of hippocampal splitting activity in 5xFAD mice, we constructed high- and low-rate trajectory spatial tuned activity curves for neurons with place fields spanning at least five stem bins. Trajectories were classified based on which correct turn (LR or RL) had higher mean peak spatial activity on the stem arm (Fig. 7A). For

example, if a neuron had a higher mean peak spatial tuned activity rate on RL trials than on LR trials along the stem arm, RL was classified as the high-rate trajectory and LR trials as the low-rate trajectory, and vice versa. Then, the differences between high- and low-rate spatial tuned curves were calculated. Significant splitting activity was identified by shuffling all correct trials identity labels by 1000 times, defining significant splitting bins as those with differences at stem bins exceeding 95% of the differences in the shuffled trials. Finally, we assessed the splitting quality between on high- and low-rate trajectory spatial activity based on these significantly splitting spatial bins.

To quantify the quality of hippocampal splitter activity, we assessed three metrics adapted from Kinsky et al (*39*) (see Methods): splitting extent, splitting discriminability and splitting reliability. Splitting extent, representing the proportion of stem bins with significant splitting activity, was reduced in 5xFAD mice (Fig. 7B, Scheirer-Ray-Hare test with the Dunn-Sidak post hoc test, AD effect: $H(1,1489) = 56.46$, $p < 0.001$; YoungCtrl *vs* YoungAD, $p < 0.0001$; OldCtrl *vs* OldAD, $p = 0.0088$;). Splitting discriminability, which quantifies the disparity between high- and low-rate trajectory tuning curves, showed an age-related decline in 5xFAD mice (Fig. 7C, AD×Age interaction effect: $H_{(1,1489)} = 11.38$, $p < 0.001$; YoungCtrl *vs* YoungAD, $p < 0.001$; OldCtrl *vs* OldAD, $p < 0.0001$). Finally, splitting reliability, measured as trial-to-trial spatial correlations on the high-rate trajectories along the stem arm, was also reduced in 5xFAD mice (Fig. 7D, AD effect: $H(1,1489) = 32.19$, $p < 0.001$; YoungCtrl *vs* YoungAD, $p < 0.001$; OldCtrl *vs* OldAD, $p < 0.001$). These metrics were also plotted along the stem arms (Fig. 7E). Furthermore, we observed a significant correlation between task performance and the Splitting Extent (Fig. 7F ; Pearson correlation, $R = 0.57$, $p = 0.001$), Discriminability ($R = 0.60$, $p = 0.0007$), Reliability ($R = 0.45$, $p = 0.013$).

Although the distribution of peak activity along the high-rate trajectories at spatial bins exhibiting splitting did not altered in 5xFAD mice (Fig. 7G, YoungCtrl *vs* YoungAD, $p = 0.988$; OldCtrl *vs* OldAD, $p = 0.639$), the onset of splitting activity was impaired (Fig. 7H). We defined onset as the first trial in which neurons exhibited splitting in at least one spatial bin. 5xFAD mice showed a delayed onset of neural splitting activity (Fig. 7H, YoungCtrl *vs.* YoungAD, $p < 0.001$; OldCtrl *vs.* OldAD, $p = 0.0068$).

To quantify the temporal progression of AD pathology on the hippocampal splitting activity, we calculated the impairment index for both young and old groups (Fig. 7I). Behavioural performance, splitting extent, discriminability, reliability, and onset trial values from 5xFAD mice were first normalised to age-matched control mice. The ratio was then subtracted from 1, so that an index of 0 indicated no significant impairment (see Table S1 for statistical details). We found that deficits in CA1 splitting quality were more pronounced than behavioural impairments in young 5xFAD mice. Although young 5xFAD mice did not exhibit a significant behavioural performance impairment index (Table S1, $p = 0.07$), several indices of splitter cell activity were already significantly impaired at this stage. Furthermore, both splitting onset and extent impairment approached their symptotic impairment levels at a young age in 5xFAD mice. Taken together, these findings suggest that degradation of hippocampal CA1 splitting activity in 5xFAD mice correlates with, and predicts, task performance deficits in the continuous alternation task.

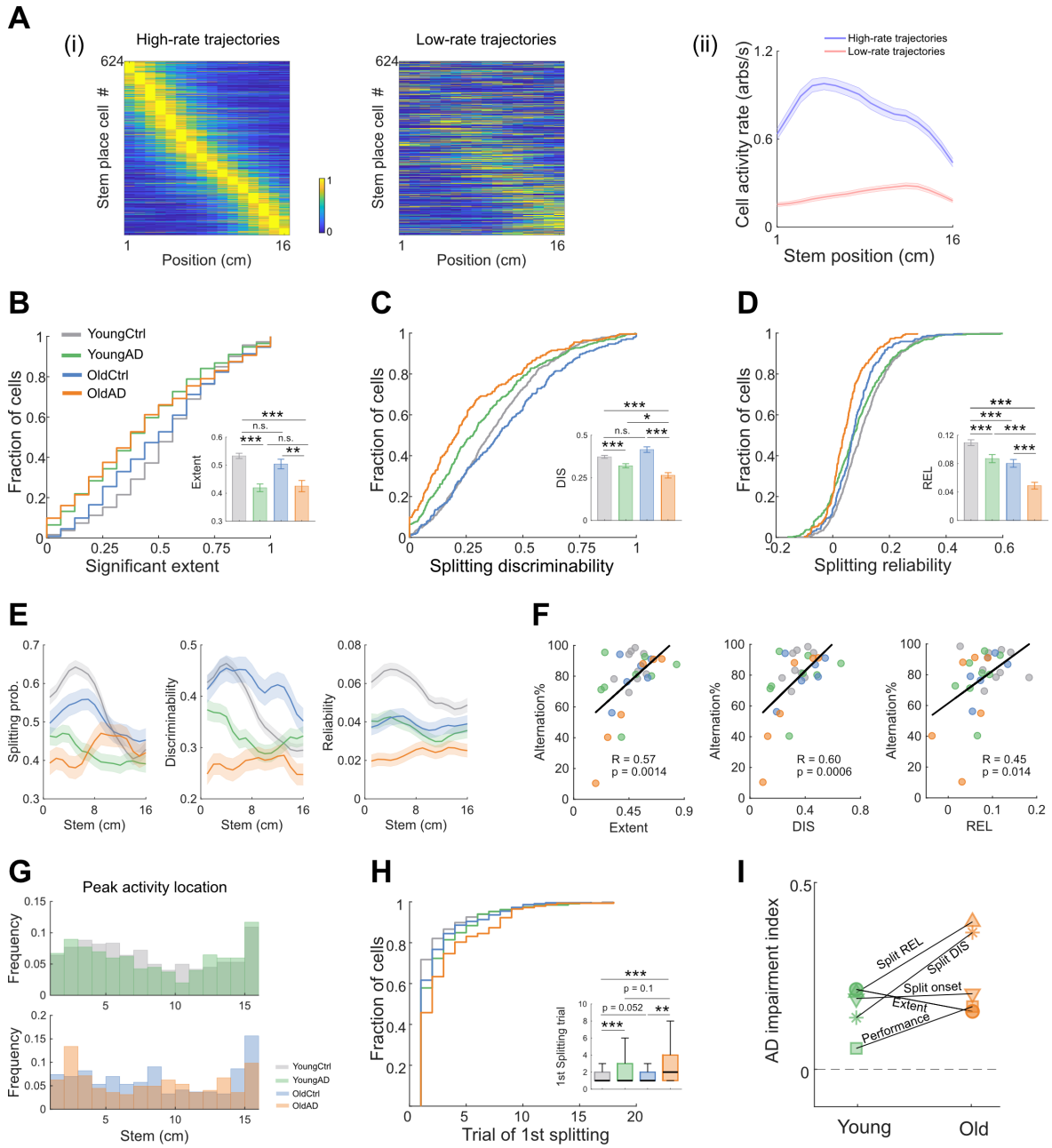

Figure 7: Quality of splitting activity is degraded in 5xFAD mice, and this correlates with behavioural performance deficits.

A. Difference in peak firing rates between left and right trajectories for CA1 cells with place fields on the stem (shown using YoungCtrl mice as an example). (i) Trajectories were classified as high or low rate based on the highest spatial peak rate. Activity was normalised to each cell's peak firing rate and sorted by field position on high-rate trajectories. Each line represents one cell. (ii) Shading indicates mean ± s.e.m. of spatial activity along the stem for high- (blue) and low-rate (red) trajectories.

B. Cumulative distribution with inset bar plots (mean ± s.e.m.) showing the proportion of stem bins with splitting activity for each neuron with place field on the stem arm.

C. As for B but for average value of discriminability splitting activity across all stem bins.

D. As for B and C but for showing the mean trial-to-trial correlation of splitting activity during high-rate trajectories across all stem bins.

E. From left to right: Shading indicates mean ± s.e.m. of the splitting probability, discriminability and reliability for each stem spatial bin across cells.

F. Correlation of splitting quality metrics with behavioural performance. For each mouse's alternation performance from left to right: splitting extent, splitting discriminability and splitting reliability.

G. Distribution of the location of peak splitting activity along the stem arm.

H. Distribution of the ordinal number of the first trial showing sustained splitting activity. Cumulative distribution with inset box plots shows the median value (± 95% CI) of first splitting trial.

I. Impairment index quantitatively showing impairments in behavioural performance, splitting extent, discriminability, reliability and onset splitting trial (1-5xFAD/Ctrl; see Table S1 for statistical details.

Data pooled across imaging sessions following behavioural training. Mice without detected stem place cells were excluded. $*$, $**$ and $***$ indicate the significance levels with the respective p values of < 0.05, < 0.01 and < 0.001.

Discussion

In this study, we introduced a novel head-fixed behavioural paradigm to assess hippocampal-associated spatial working memory. This paradigm allowed us to examine how Alzheimer's disease-related amyloid pathology affects both behavioural performance and hippocampal neuronal spatial representations, by two-photon in vivo imaging in 5xFAD mice during a continuous spatial alternation task. Previous research has established that the 5xFAD mouse begins to develop amyloid deposits between 2 to 4 months of age, with intraneuronal accumulation of Aβ42 starting as early as 1.5 months (*28*) . This amyloid burden in 5xFAD mice intensifies over their lifespan (*28, 40*). By 4 to 6 months, these mice exhibit substantial amyloid deposition alongside observed deficits in synaptic transmission, LTP, and sharp wave-ripple events (*28, 31, 41, 42*). While some studies have detected mild impairments in spatial or hippocampus-independent memory as early as 3 to 4 months, more pronounced memory deficits become evident at later stages, beyond 4–6 months of age (*30, 43, 44*). Consistent with these findings, our study observed mild behavioural cognitive deficits in young 5xFAD mice (2–4 months) during the head-fixed alternation task, whereas old 5xFAD mice (7 to 12 months) displayed significant spatial memory impairments (Fig. 2B, C, Fig. S3E).

Behavioural hyperactivity was observed in 5xFAD mice (Fig. 2F, G), consistent with previous studies using the open field test, rotarod test, home-cage wheel-running assessments and actimetry (*45, 46*). These findings suggest that the reduced alternation percentages in old 5xFAD mice were not due to a lack of environmental exploration. Our findings align with previous studies indicating that neuronal hyperactivity (Fig. S2 C, D) and disrupted neural spatial representations (Fig. 3) occur in both mouse model of AD and human sporadic AD (*47, 48*). Furthermore, our observation of disrupted speed modulation of CA1 neuronal activity in our study is particularly relevant (Fig. F, G), as local field potential oscillations in theta and gamma frequencies are closely linked to running speed (*49, 50*). Future research could build upon these findings by investigating the coherence between hippocampal oscillations, neuronal calcium activity, running speed, and behavioural cognitive performance.

Furthermore, our findings revealed reduced spatial information, a lower proportion of place cells, and decreased stability in spatial coding (Fig. 3), consistent with previous studies demonstrating a decline in hippocampal neural spatial representations in mouse models of AD (*13-15*). However, in our results, while young 5xFAD exhibited only mild behavioural performance impairments (Fig. 2B, C), they still demonstrated significantly disrupted spatial representations in the head-fixed alternation task. Hence, our results indicate that deficits in place cell encoding are more pronounced than alternation performance deficits in young 5xFAD mice (Fig. 3). This suggests that substantial impairments in neural spatial representations may precede and predict the onset of cognitive behavioural symptoms in these mice. Furthermore, these deficits in place cell encoding may be associated with the reduced long-term potentiation (LTP) and impaired synaptic transmission previously reported in 5xFAD mice of a similar age (*41, 42*).

The stabilisation of place cell coding is thought to be linked to the high memory demand and attentional engagement required in memory-guided tasks (*51, 52*). In our task, the trial-to-trial stability of place cell activity was found to diminish in 5xFAD mice (Fig. 3E-G), suggesting difficulties in consistently reactivating place cells within short intervals between trials. Thus, old 5xFAD mice may fail to allocate sufficient attention or integrate sensory,

visual, and auditory stimuli into spatial memory coding during the alternation task. However, although fewer place cells in 5xFAD mice maintained consistent spatial tuning throughout the learning period, the observed session-to-session stability in spatial encoding suggests that long-term spatial memory may be relatively preserved (Fig. 4) or subject to a different impairment mechanism, requiring further investigation.

We observed an age-related decline in spatially tuned activity around reward locations, indicating a specific vulnerability of reward-related spatial learning in 5xFAD (Fig. 5). Memory recall of reward locations provides essential spatial cues for goal directed task (*53*), as rewards enhance motivation, navigation, and attentional engagement. Reduced attention, a hallmark of AD (53), may reduce task engagement in 5xFAD mice, weakening hippocampal spatial representation (52). Reward encoding relies on sensory input, activating dopaminergic circuit that influence hippocampal cognitive function and synaptic plasticity via the ventral tegmental area (VTA). While we did not assess dopaminergic deficits, they are observed in mild cognitive impairment (MCI) and AD patients with neuropsychiatric symptoms (*54, 55*).

Recent studies suggest that the hippocampal supports cognitive process beyond spatial representations (*56-58*). Our findings provide insights into both spatial and non-spatial cognitive impairments in hippocampal neurons within a single behavioural task designed to assess cognitive dysfunction. Our study presents the first report of hippocampal splitter cells in a mouse model of AD (Fig. 6). Splitter cells play a crucial role in encoding past experiences and future decisions, integrating within the prefrontal-thalamo-hippocampal circuit that underpins spatial navigation (*38*). We observed a positive correlation between the proportion of hippocampal splitter cells and alternation performance in mice (Fig. 6 C, D). Further analysis of the quality of splitting activity (trajectory-dependent activity) revealed significant degradation in 5xFAD mice (Fig. 7B-D, H), which was associated with their behavioural performance deficits (Fig. 7F). Moreover, the degradation of splitting activity may predict behavioural impairments in 5xFAD mice (Fig. 7I).

This splitting activity dysfunctionality may share underlying neuronal mechanisms with place cells deficits. Generation of splitter cells likely requires recruitment of more complex and highly integrated neural networks, as well as greater synaptic plasticity. Given that synaptic plasticity can convert silent CA1 neurons into splitter cells (*25*), and that synaptic transmission is impaired in 5xFAD mice (*41, 42*), impaired synaptic function may contribute to deficits in both spatial and contextual neuronal representations. Overall, our findings imply a link between the dysfunction of hippocampal splitting activity and cognitive impairment in the early stages of AD. Future studies could refine the task paradigm to investigate whether prospective or retrospective splitter cell activity is altered in AD (*59*), providing a further detailed understanding of neural network impairments.

Limitations of the study

First, we did not account for sex differences in our analysis. Human studies indicate that AD prevalence and severity are higher in females, with sex-specific differences observed in amyloid pathology and cognitive decline (*60, 61*). Similar patterns have been reported in the 5xFAD model, with female mice exhibiting greater amyloid deposition and potentially distinct cognitive impairments compared to males (*45, 62-64*). Second, although calcium imaging is a powerful tool for assessing neuronal activity, potential discrepancies in calcium indicator dynamics in AD models must be considered. Variations in calcium indicator

expression, deregulation of calcium signalling, and altered decay kinetics in 5xFAD mice could affect the accuracy of spike inference (*65*). Third, incorporating pupil and lick tracking could provide further insights into attention and task engagement, thereby clarifying the mechanisms underlying the observed behavioural impairments. Finally, our cognitive assessment was limited to a single behavioural task. The task described here does not include an explicit or variable delay period, instead depending upon the time taken for the mouse to return to the decision point. Incorporation of a delay period, for instance via a servomotor actuation mechanism, which is feasible but beyond the scope of the present study, would potentially make the task more dependent upon the hippocampus, according to results from freely moving animals (*37*).

Materials and Methods

Experimental Animals

5xFAD mice express human APP and PSEN1 transgenes with a total of five AD-linked mutations: the Swedish (K670N/M671L), Florida (I716V), and London (V717I) mutations in APP, and the M146L and L286V mutations in PSEN1. Male hemizygous 5xFAD mice (B6SJL-Tg (APPSwFILon, PSEN1∗M146L∗L286V) 6799Vas/Mmjax, JAX stock # 034840) were crossed with female homozygous Chat-IRES-Cre(∆neo) mice (JAX stock # 031661 on a C57BL/6J genetic background) to maintain the 5xFAD positive ($5xFAD^{+}$/Chat-Cre^{+} as 5xFAD group) and non-5xFAD ($5xFAD^{-}$/Chat-Cre^{+} as control group) mice. Two 5xFAD positive mice (one young and one old) contributed data and were derived from a crossing between the (B6SJL-Tg (APPSwFILon, PSEN1∗M146L∗L286V) 6799Vas/Mmjax, JAX stock # 034840) with C57BL/6J (JAX stock # 000664). Colonies under standard animal breeding at Imperial College London. The animal room was kept on a reverse 12:12 light-dark cycle daily.

Ear samples were collected from 5xFAD-Tg and Non-5xFAD-Tg transgenic littermates for genotyping identification. Real-time PCR was used for genotyping 5xFAD transgenic with probes APPswTg and huPSEN1Tg, conducted by Transnetyx company. Animals were divided into two age groups: young group aged (young control age = 3.6 months, N=10; young AD median age = 3.8 months, N=8) and old group aged (old control median age = 8.6 months, N=6, old AD median age = 8.2 months, N=7). Non-AD transgenic littermates were used as controls. Both male and female mice were used for this study. All experimental procedures were carried out under the Animals (Scientific Procedures) Act 1986 and according to Home Office and institutional guidelines, under a Project License to SR Schultz.

Surgeries

Mice were anaesthetised with 1.5-3% isoflurane (Iso-Vet, Chanelle Pharma) and body temperature was maintained at 37°C. Analgesia was administered pre-operatively with Carprofen (5 mg/kg SC, Rimadyl, Zoetis) and Buprenorphine (0.07 mg/kg SC, Vetergesic, Ceva Animal Health Ltd). Anaesthetic depth was monitored every 10 minutes via the pedal flexion reflex. A small (0.5 mm) craniotomy was performed and 1 µl of a viral cocktail containing two adeno-associated viruses (pGP-AAV-syn-jGCaMP7s-WPRE, Addgene catalogue 104487-AAV9; pAAV-CAG-tdTomato, Addgene catalogue 59462-AAV9) in a 3:1 ratio was injected into the hippocampal CA1 region (coordinates from bregma, in mm:

-1.3 and -1.5 DV, -1.8 ML, -2.0 AP). Ten minutes after viral injection, a 3-mm circular craniotomy was made, and the overlying cortex (including parietal cortex and parts of visual and hindlimb sensory cortex) was aspirated using a 27-gauge needle connected to a water pump until the corpus callosum fibres were exposed. A stainless-steel cannula (3 mm diameter, 1.5mm height) with a glass bottom was inserted and secured with histoacryl glue (B. Braun Surgical). The hippocampal imaging window was described by Dombeck et al. (*66*). A stainless-steel head plate (8.5 mm aperture) was glued to the skull, centred over the craniotomy. The exposed skull outside the head plate aperture was covered with dental cement mixed with black powder paint. Postoperatively, mice received Carprofen (5 mg/kg/24 hrs) in oral water for three days. Behavioural training began after a 2-3 week recovery period.

Behavioural training in head-fixed mice

Maze apparatus

We used a carbon fibre maze with attached visual and tactile cues, floating on the Neurotar tracker air table (Mobile HomeCage, Neurotar). Built-in magnets in maze allowed for tracking the animal's position within the environment. The maze has a diameter of 32.5 cm, with a 16 cm-long stem arm (start arm). The corridor width for all arms was 5 cm. Visual cues were provided by attached phosphorescent tape, and tactile cues were added using Fiberglass Mesh Tape on the inner wall of the maze. The training cage tape was fully charged with daylight before the commencement of any training sessions.

Handling and habituation

Acclimatization to both the room and maze is essential for mice to become familiar with the training environment prior to official training sessions. Mice were handled at least two days before behavioural training. On the day before training began, mice freely explored the air-lifted T maze in the training room under red lighting for 10 minutes. During the first 5 training days, mice were allowed 5 minutes of free exploration before head fixation.

Spatial continuous rewarded alternation task

To assess goal directed, hippocampal-dependent spatial memory in the head-fixed mice, we trained them on a spatial continuous rewarded alternation task. To motivate task engagement, mice were subjected to water restriction prior to the first day of training. After 5 days, their body weight typically stabilised at 85 to 90% of initial body weight, with each mouse receiving a minimum of 1.5 ml of water per day. If the full daily water ration was not received during the task training, supplementary water was provided in the home cage after the second session to maintain body weight above 85%. Mice were trained in the dark during the learning of the alternation task. For the first trial, mice could freely choose reward arm. A 4 µl reward was delivered via a lick spout attached to the head-plate clamp and controlled by a peristaltic pump (Campden Instruments), accompanied by a beep. In subsequent trials, a reward was only delivered when mouse entered the reward arm opposite to the one visited in the previous trial. A complete trial required the mouse to pass through the previous trial reward position, return arm, centre arm (stem arm), choice arm, and arrive at the next reward location. Head-fixed animals were trained for 45 minutes each session twice a day, with at least 4 hours between sessions. From the 6th training day onward, 1% sucrose water was used as the reward during training and imaging sessions, but still supplied

water for supplementary fluid. Mouse position and behavioural data were recorded using the Neurotar Mobile HomeCage tracker (V3.0.0.64). The figure-8 maze was cleaned with 70% ethanol before each mouse training or imaging recording.

In vivo two-photon Ca^{2+} imaging

Two-photon calcium imaging was conducted using a Scientifica resonant scanning microscope with a 16× Nikon water-immersion objective (LWD 0.8 NA). jGCamp7s and tdTomato fluorophores were excited at 940 nm using Ti:Sapphire laser (Mai Tai HP, Newport). The 50% (vol%) ultrasound gel was used as the immersion medium. Images (490 × 490 μm, 512 × 512 pixels) were acquired at 30.9 Hz frame rate using SciScan 1.3 software. Imaging was synchronized with behaviour recording via a start TTL signal sent from the behaviour recording software Neurotar. All mice underwent imaging afterwards 10th training day. Additionally， some mice were also imaged on 6th and 8th training days to enable imaging across the learning period. Each imaging session lasted no longer than two hours per mouse per day. At the beginning of each session, mice were head-fixed at the stem arm and restricted by two carbon fibre doors. Once the targeted field of view (FOV) was located, the doors were removed and imaging commenced as the mouse began running. To ensure sufficient data for spatial tuning analyses, a minimum of 80 total trials was required for each imaging session, though approximately 100 trials were usually recorded per session.

Quantification and statistical analysis

Behaviour data analysis

Alternation performance： Only complete trials (see behaviour training) were included in the analysis. As mice received a reward on their initial free choice, this first choice was excluded from the calculation of correct trials. Alternation performance was defined as the percentage of correct trials out of the total number of trials.

Trajectory linearisation: To linearise the mouse trajectory, the maze was segmented into four functional zones: the return arm, stem arm, choice arm and reward arm. Trajectories were parsed accordingly, starting from the return arm, then moving up the stem arm into the choice arm, and ending in the reward arm. The reward spout marked the boundary between the choice and reward arms. Each trajectory was then categorised into LR, RL, LL and RR trial types based on maze segmentation. Linearised trajectories were mapped by trial type onto a standardised 49.5 cm track, corresponding to the estimated length of a complete trial. Trials were chronologically ordered based on the sequence of completion in the maze (see Supplementary Fig. 1).

Imaging data processing

To extract calcium activity from individual neurons, we employed a customised image processing pipeline based on the CaImAn MATLAB package (*67*), following the protocol described by Go et al. (*20*). Imaging data were initially corrected for motion artefacts using sequential rigid and non-rigid registration methods, aligning frames a reference template from the same imaging session. Regions of interest (ROIs) were then identified, with excluding any overlapping ROIs. To enable tracking of ROIs across multiple sessions, images from different sessions were registered to a template from one session, and ROIs

were identified on a temporally concatenated video. For quantification of single-neuron calcium amplitude trains, neural activity was deconvolved using a sparse non-negative deconvolution approach. This was implemented with an exponential kernel corresponding to the decay timescale of the calcium indicator employed, utilizing the OASIS (Online Active Set method to Infer Spikes) algorithm to infer fluorescence activity into calcium trains with both onset times and amplitudes.

To eliminate out any discrepancies in OASIS event amplitude between different mice and FOVs, we fitted the distribution of event amplitudes for each FOV in each mouse to a lognormal distribution and standardised the distribution for each FOV to unit mean. This eliminates variability in event amplitude due to differences in signal to noise ratio (for instance due to imaging depth and viral expression), and makes it possible to compare calcium activity rates objectively across FOVs and animals. The resulting deconvolved calcium event amplitudes are expressed in consistent arbitrary units across the entire dataset.

Place cell identification

The Figure-8 maze was discretized into 1 cm-wide bins, forming a 32 × 32 grid, to construct spatial rate maps. For each bin, we calculated the spatial activity rate by dividing the sum of the standardised deconvolved calcium amplitudes collected from that bin by the total time the mouse spent in that bin, only including running speeds larger than 8 mm/s. We employed a Gaussian kernel with a sigma value of [3,3] to smooth the spatial rate maps. The spatial information content of each neuron was calculated using Skaggs's spatial information method (*68*) (bits per arb, standardised amplitude rate), is calculated using the following formula:

$$\mathrm{SI} = \sum_{i=1}^{N} P_i \frac{\lambda_i}{\lambda} log_2\left(\frac{\lambda_i}{\lambda}\right)$$

where SI is the spatial information in bits/arb. P_i is the probability of the mouse being in the i-th bin. λ_i is the mean standardised amplitude rate of the cell when the mouse in the *i*-th bin. λ is the overall mean standardised amplitude rate of the cell across the entire environment. N is the total number of spatial bins. 2D place cells within the Figure-8 maze were identified based on the following criteria: 1) A neuron's SI must exceed the 95th percentile of the shuffled SI values. 2) the neuron should be active within the place field for more than 2% of the time the mouse spends in that field. 3) the size of the place field must exceed 5 cm^2. The boundary of a place field was determined by encompassing all connected occupancy bins where the smoothed rate amplitude was at least 50% of the peak rate in the occupancy bin. For 1D place cells selection, we calculated for total, RL, LR, LL and RR trials respectively. The criterions for 1D place cells in linearised trajactory: 1) spatial information need to in the top of 5 % shuffled spatial information. 2) cells active time percent of time spent in place field should be at least 1 %. 3) cells active more than 30% of total number of trials.

Splitter cell identification

To identify hippocampal splitter cells, the stem arm of the figure-8 maze was first divided into 1 cm spatial bins. Place cells with place fields spanning at least five spatial bins along the stem were selected for analysis. For each cell, the neural activity rate was calculated at each stem bin across trials. Spatial tuned curves were constructed separately for correct left-turn and right-turn trials, and the differences between these curves at each stem bins were calculated. Splitter cells were identified through a permutation procedure, involving 1000

random shuffles of left- and right-turn trials labels. A significant splitter cell was defined as a neuron with place fields in at least five stem arm bins, and with tuning curve differences in at least five of those bins exceeding the 95th percentile of the shuffled trial results.

Linear discriminant analysis (LDA)

A linear discriminant decoder was trained using data from a randomly selected 70% of trials in each imaging session. The decoder was implemented using MATLAB's built-in function fitcdiscr, with the discrimination type set to 'pseudolinear'. The calcium activity of each neuron at each time point while the mouse was on the stem arm served as the input variables, and the mouse's upcoming turn direction was used as the response variable. Only correct trials (left-right and right-left) were included for both training and testing. The trained decoder was then applied to predict the turn direction on the remaining 30% of correct trials. This procedure was repeated 1,000 times with different random subsets of trials used for training and testing. Decoding accuracy was computed in 1 cm spatial bins along the stem arm, and the mean decoding accuracy was defined as the average accuracy across all bins within a given session.

Trajectory-dependent activity quality

The quality of trajectory-dependent neuronal activity was characterised using three metrics , applied to the analysis of cells with place fields located along the stem arm (*39*). Splitting extent was defined as the proportion of stem bins that demonstrated a statistically significant disparity between the left and right spatial tuned curves, as determined by a permutation test involving 1000 random shuffles of trial identities. A bin was deemed as a splitting bin if the observed difference exceeded the 95th percentile of differences obtained from the shuffled distribution. Discriminability was quantified by summing the absolute values of the differences between left and right tuning curves across all stem bins, and dividing by the total sum of activity in both direction tuned curves across all stem bins. Reliability quantifies the consistency of trial-to-trial of spatial correlations in a neuron's preferred turning direction across trials along the stem arm. Trial-to-trial correlations for splitting activity were computed using the Spearman correlation coefficients between the spatial activity of adjacent preferred tuning direction trials within the same imaging session. For instance, if a neuron exhibited splitting activity along the stem arm bins and showed a preferred firing direction during left-right (L-R) trials, trial-to-trial correlations were calculated between the spatial tuned activity of adjacent L-R trials.

Statistical tests

Data were presented as mean ± SEM unless otherwise specified. All analyses and visualisations were performed using MATLAB. The normality of data distribution was assessed using the Shapiro-Wilk test, and the homogeneity of variance was evaluated by Levene's test. When both assumptions were met, data were analysed using two-tailed Student's t tests, one or two-way ANOVA followed by the Tukey-kramer post hoc test for multiple comparisons. If normality and homogeneity of variance were not met, the Mann-Whitney U test was used for two-sample comparisons, and the Scheirer-Ray-Hare test with the Dunn-Sidak post hoc test was applied for multiple comparisons with two factors. The significance levels was set at $p \leq 0.05$.

Acknowledgments

We thank Yu Liu and Nawal Zabouri for their help with animal genotyping and daily support, Jina Song for assisting with the behavioural training protocol, and Seigfred Prado for his help with image processing using high-performance computing.

Funding:
Mrs Anne Uren and the Michael Uren Foundation to SRS
EPSRC EP/W024020/1 and EP/W035057/1 to SRS
BBSRC BB/Y514202/1 to SRS
CZI CP-2-1-Schultz to SRS
China Scholarship Council CSC scholarship to YL

Author contributions:
Y.L. and S.R.S. conceived and designed the study. Y.L.mainly conducted experiments and collected data under guidance and supervision of S.R.S. and M.A.G., Y.L. and H.Z. analyzed data. M.A.G. and H.Z. contributed to imaging data processing. Y.L. and S.R.S. wrote the paper. All authors discussed and commented on the manuscript.

Competing interests: Authors declare that they have no competing interest.

Data and materials availability: Code and data used to generate the figures described in this paper will be made available via DataDryad at the time of publication, with a DOI to be included here.

References

1. A. A. Tahami Monfared, M. J. Byrnes, L. A. White, Q. Zhang, Alzheimer's Disease: Epidemiology and Clinical Progression. *Neurol Ther* **11**, 553-569 (2022).
2. M. A. Busche, B. T. Hyman, Synergy between amyloid-β and tau in Alzheimer's disease. *Nature Neuroscience* **23**, 1183-1193 (2020).
3. H. Xiong, D. Callaghan, A. Jones, D. G. Walker, L.-F. Lue, T. G. Beach, L. I. Sue, J. Woulfe, H. Xu, D. B. Stanimirovic, Cholesterol retention in Alzheimer's brain is responsible for high β-and γ-secretase activities and Aβ production. *Neurobiology of disease* **29**, 422-437 (2008).
4. C. Condello, P. Yuan, A. Schain, J. Grutzendler, Microglia constitute a barrier that prevents neurotoxic protofibrillar Aβ42 hotspots around plaques. *Nat. Commun.* **6**, 6176 (2015).
5. B. Bellaver, G. Povala, P. C. Ferreira, J. P. Ferrari-Souza, D. T. Leffa, F. Z. Lussier, A. L. Benedet, N. J. Ashton, G. Triana-Baltzer, H. C. Kolb, Astrocyte reactivity influences amyloid-β effects on tau pathology in preclinical Alzheimer's disease. *Nature medicine* **29**, 1775-1781 (2023).
6. S. Frere, I. Slutsky, Alzheimer's Disease: From Firing Instability to Homeostasis Network Collapse. *Neuron* **97**, 32-58 (2018).
7. J. Hort, J. Laczó, M. Vyhnálek, M. Bojar, J. Bureš, K. Vlček, Spatial navigation deficit in amnestic mild cognitive impairment. *Proceedings of the National Academy of Sciences* **104**, 4042-4047 (2007).
8. C. Newton, M. Pope, C. Rua, R. Henson, Z. Ji, N. Burgess, C. T. Rodgers, M. Stangl, M. E. Dounavi, A. Castegnaro, I. Koychev, P. Malhotra, T. Wolbers, K. Ritchie, C. W.

Ritchie, J. O'Brien, L. Su, D. Chan, P. D. R. Programme, Entorhinal-based path integration selectively predicts midlife risk of Alzheimer's disease. *Alzheimers Dement* **20**, 2779-2793 (2024).

9. T. Hope, K. M. Tilling, K. Gedling, J. M. Keene, S. D. Cooper, C. G. Fairburn, The structure of wandering in dementia. *International Journal of Geriatric Psychiatry* **9**, 149-155 (1994).
10. Y. Vyas, J. M. Montgomery, J. E. Cheyne, Hippocampal deficits in amyloid-β-related rodent models of Alzheimer's disease. *Frontiers in neuroscience* **14**, 266 (2020).
11. M. J. West, P. D. Coleman, D. G. Flood, J. C. Troncoso, Differences in the pattern of hippocampal neuronal loss in normal ageing and Alzheimer's disease. *The lancet* **344**, 769-772 (1994).
12. E. J. Mufson, L. Mahady, D. Waters, S. E. Counts, S. E. Perez, S. DeKosky, S. D. Ginsberg, M. D. Ikonomovic, S. Scheff, L. Binder, Hippocampal plasticity during the progression of Alzheimer's disease. *Neuroscience* **309**, 51-67 (2015).
13. F. Cacucci, M. Yi, T. J. Wills, P. Chapman, J. O'Keefe, Place cell firing correlates with memory deficits and amyloid plaque burden in Tg2576 Alzheimer mouse model. *Proceedings of the National Academy of Sciences* **105**, 7863-7868 (2008).
14. R. Zhao, S. W. Fowler, A. C. Chiang, D. Ji, J. L. Jankowsky, Impairments in experience-dependent scaling and stability of hippocampal place fields limit spatial learning in a mouse model of Alzheimer's disease. *Hippocampus* **24**, 963-978 (2014).
15. A. J. Mably, B. J. Gereke, D. T. Jones, L. L. Colgin, Impairments in spatial representations and rhythmic coordination of place cells in the 3xTg mouse model of Alzheimer's disease. *Hippocampus* **27**, 378-392 (2017).
16. X. Lin, L. Chen, D. Baglietto-Vargas, P. Kamalipour, Q. Ye, F. M. LaFerla, D. A. Nitz, T. C. Holmes, X. Xu, Spatial coding defects of hippocampal neural ensemble calcium activities in the triple-transgenic Alzheimer's disease mouse model. *Neurobiology of disease* **162**, 105562 (2022).
17. H. Jun, A. Bramian, S. Soma, T. Saito, T. C. Saido, K. M. Igarashi, Disrupted place cell remapping and impaired grid cells in a knockin model of Alzheimer's disease. *Neuron* **107**, 1095-1112. e1096 (2020).
18. P. Ravassard, A. Kees, B. Willers, D. Ho, D. A. Aharoni, J. Cushman, Z. M. Aghajan, M. R. Mehta, Multisensory control of hippocampal spatiotemporal selectivity. *Science* **340**, 1342-1346 (2013).
19. Z. M. Aghajan, L. Acharya, J. J. Moore, J. D. Cushman, C. Vuong, M. R. Mehta, Impaired spatial selectivity and intact phase precession in two-dimensional virtual reality. *Nat Neurosci* **18**, 121-128 (2015).
20. M. A. Go, J. Rogers, G. P. Gava, C. E. Davey, S. Prado, Y. Liu, S. R. Schultz, Place cells in head-fixed mice navigating a floating real-world environment. *Frontiers in cellular neuroscience* **15**, 618658 (2021).
21. E. R. Wood, P. A. Dudchenko, R. J. Robitsek, H. Eichenbaum, Hippocampal neurons encode information about different types of memory episodes occurring in the same location. *Neuron* **27**, 623-633 (2000).
22. L. M. Frank, E. N. Brown, M. Wilson, Trajectory encoding in the hippocampus and entorhinal cortex. *Neuron* **27**, 169-178 (2000).
23. E. Duvelle, R. M. Grieves, M. A. A. van der Meer, Temporal context and latent state inference in the hippocampal splitter signal. *Elife* **12**, (2023).
24. P. F. Chapman, G. L. White, M. W. Jones, D. Cooper-Blacketer, V. J. Marshall, M. Irizarry, L. Younkin, M. A. Good, T. V. Bliss, B. T. Hyman, S. G. Younkin, K. K. Hsiao, Impaired synaptic plasticity and learning in aged amyloid precursor protein transgenic mice. *Nat Neurosci* **2**, 271-276 (1999).

25. X. Zhao, C. L. Hsu, N. Spruston, Rapid synaptic plasticity contributes to a learned conjunctive code of position and choice-related information in the hippocampus. *Neuron* **110**, 96-108 e104 (2022).
26. S. M. Kim, L. M. Frank, Hippocampal lesions impair rapid learning of a continuous spatial alternation task. *PLoS One* **4**, e5494 (2009).
27. R. Gerlai, A new continuous alternation task in T-maze detects hippocampal dysfunction in mice. A strain comparison and lesion study. *Behav Brain Res* **95**, 91-101 (1998).
28. H. Oakley, S. L. Cole, S. Logan, E. Maus, P. Shao, J. Craft, A. Guillozet-Bongaarts, M. Ohno, J. Disterhoft, L. Van Eldik, Intraneuronal β-amyloid aggregates, neurodegeneration, and neuron loss in transgenic mice with five familial Alzheimer's disease mutations: potential factors in amyloid plaque formation. *Journal of Neuroscience* **26**, 10129-10140 (2006).
29. M. S. Pádua, J. L. Guil-Guerrero, P. A. Lopes, Behaviour Hallmarks in Alzheimer's Disease 5xFAD Mouse Model. *International Journal of Molecular Sciences* **25**, 6766 (2024).
30. S. D. Girard, M. Jacquet, K. Baranger, M. Migliorati, G. Escoffier, A. Bernard, M. Khrestchatisky, F. Féron, S. Rivera, F. S. Roman, Onset of hippocampus-dependent memory impairments in 5XFAD transgenic mouse model of Alzheimer's disease. *Hippocampus* **24**, 762-772 (2014).
31. R. Kimura, M. Ohno, Impairments in remote memory stabilization precede hippocampal synaptic and cognitive failures in 5XFAD Alzheimer mouse model. *Neurobiology of disease* **33**, 229-235 (2009).
32. L. Devi, M. Ohno, Cognitive benefits of memantine in Alzheimer's 5XFAD model mice decline during advanced disease stages. *Pharmacol Biochem Behav* **144**, 60-66 (2016).
33. T. Wang, Y. Chen, Y. Zou, Y. Pang, X. He, Y. Chen, Y. Liu, W. Feng, Y. Zhang, Q. Li, Locomotor hyperactivity in the early-stage Alzheimer's disease-like pathology of APP/PS1 mice: associated with impaired polarization of astrocyte aquaporin 4. *Aging and Disease* **13**, 1504 (2022).
34. B. Kim, G. O. Noh, K. Kim, Behavioural and psychological symptoms of dementia in patients with Alzheimer's disease and family caregiver burden: a path analysis. *BMC geriatrics* **21**, 1-12 (2021).
35. C. Lever, T. Wills, F. Cacucci, N. Burgess, J. O'Keefe, Long-term plasticity in hippocampal place-cell representation of environmental geometry. *Nature* **416**, 90-94 (2002).
36. Y. Ziv, L. D. Burns, E. D. Cocker, E. O. Hamel, K. K. Ghosh, L. J. Kitch, A. El Gamal, M. J. Schnitzer, Long-term dynamics of CA1 hippocampal place codes. *Nat Neurosci* **16**, 264-266 (2013).
37. J. A. Ainge, M. A. van der Meer, R. F. Langston, E. R. Wood, Exploring the role of context-dependent hippocampal activity in spatial alternation behavior. *Hippocampus* **17**, 988-1002 (2007).
38. H. T. Ito, S. J. Zhang, M. P. Witter, E. I. Moser, M. B. Moser, A prefrontal-thalamo-hippocampal circuit for goal-directed spatial navigation. *Nature* **522**, 50-55 (2015).
39. N. R. Kinsky, W. Mau, D. W. Sullivan, S. J. Levy, E. A. Ruesch, M. E. Hasselmo, Trajectory-modulated hippocampal neurons persist throughout memory-guided navigation. *Nat Commun* **11**, 2443 (2020).
40. K. L. Youmans, L. M. Tai, T. Kanekiyo, W. B. Stine Jr, S.-C. Michon, E. Nwabuisi-Heath, A. M. Manelli, Y. Fu, S. Riordan, W. A. Eimer, Intraneuronal Aβ detection in 5xFAD mice by a new Aβ-specific antibody. *Molecular neurodegeneration* **7**, 1-14 (2012).

41. S. Forner, S. Kawauchi, G. Balderrama-Gutierrez, E. A. Kramar, D. P. Matheos, J. Phan, D. I. Javonillo, K. M. Tran, E. Hingco, C. da Cunha, N. Rezaie, J. A. Alcantara, D. Baglietto-Vargas, C. Jansen, J. Neumann, M. A. Wood, G. R. MacGregor, A. Mortazavi, A. J. Tenner, F. M. LaFerla, K. N. Green, Systematic phenotyping and characterization of the 5xFAD mouse model of Alzheimer's disease. *Sci Data* **8**, 270 (2021).
42. N. Crouzin, K. Baranger, M. Cavalier, Y. Marchalant, C. Cohen-Solal, F. S. Roman, M. Khrestchatisky, S. Rivera, F. Feron, M. Vignes, Area-specific alterations of synaptic plasticity in the 5XFAD mouse model of Alzheimer's disease: dissociation between somatosensory cortex and hippocampus. *PLoS One* **8**, e74667 (2013).
43. A. J. Martorell, A. L. Paulson, H.-J. Suk, F. Abdurrob, G. T. Drummond, W. Guan, J. Z. Young, D. N.-W. Kim, O. Kritskiy, S. J. Barker, Multi-sensory gamma stimulation ameliorates Alzheimer's-associated pathology and improves cognition. *Cell* **177**, 256-271. e222 (2019).
44. H. Zhang, L. Chen, K. G. Johnston, J. Crapser, K. N. Green, N. M.-L. Ha, A. J. Tenner, T. C. Holmes, D. A. Nitz, X. Xu, Degenerate mapping of environmental location presages deficits in object-location encoding and memory in the 5xFAD mouse model for Alzheimer's disease. *Neurobiology of disease* **176**, 105939 (2023).
45. A. L. Oblak, P. B. Lin, K. P. Kotredes, R. S. Pandey, D. Garceau, H. M. Williams, A. Uyar, R. O'Rourke, S. O'Rourke, C. Ingraham, D. Bednarczyk, M. Belanger, Z. A. Cope, G. J. Little, S. G. Williams, C. Ash, A. Bleckert, T. Ragan, B. A. Logsdon, L. M. Mangravite, S. J. Sukoff Rizzo, P. R. Territo, G. W. Carter, G. R. Howell, M. Sasner, B. T. Lamb, Comprehensive Evaluation of the 5XFAD Mouse Model for Preclinical Testing Applications: A MODEL-AD Study. *Front Aging Neurosci* **13**, 713726 (2021).
46. L. Gephine, C. M. Roux, T. Freret, M. Boulouard, M. Leger, Vulnerability of Spatial Pattern Separation in 5xFAD Alzheimer's Disease Mouse Model. *J Alzheimers Dis* **97**, 1889-1900 (2024).
47. A. M. Miranda, M. Herman, R. Cheng, E. Nahmani, G. Barrett, E. Micevska, G. Fontaine, M.-C. Potier, E. Head, F. A. Schmitt, Excess synaptojanin 1 contributes to place cell dysfunction and memory deficits in the aging hippocampus in three types of Alzheimer's disease. *Cell reports* **23**, 2967-2975 (2018).
48. M. A. Busche, X. Chen, H. A. Henning, J. Reichwald, M. Staufenbiel, B. Sakmann, A. Konnerth, Critical role of soluble amyloid-beta for early hippocampal hyperactivity in a mouse model of Alzheimer's disease. *Proc Natl Acad Sci U S A* **109**, 8740-8745 (2012).
49. L. L. Colgin, Rhythms of the hippocampal network. *Nature Reviews Neuroscience* **17**, 239-249 (2016).
50. T. Ridler, J. Witton, K. G. Phillips, A. D. Randall, J. T. Brown, Impaired speed encoding and grid cell periodicity in a mouse model of tauopathy. *Elife* **9**, e59045 (2020).
51. R. Zemla, J. J. Moore, M. D. Hopkins, J. Basu, Task-selective place cells show behaviorally driven dynamics during learning and stability during memory recall. *Cell reports* **41**, (2022).
52. C. G. Kentros, N. T. Agnihotri, S. Streater, R. D. Hawkins, E. R. Kandel, Increased attention to spatial context increases both place field stability and spatial memory. *Neuron* **42**, 283-295 (2004).
53. M. Sosa, L. M. Giocomo, Navigating for reward. *Nat Rev Neurosci* **22**, 472-487 (2021).
54. X. Pan, A. C. Kaminga, S. W. Wen, X. Wu, K. Acheampong, A. Liu, Dopamine and dopamine receptors in Alzheimer's disease: a systematic review and network meta-analysis. *Frontiers in aging neuroscience* **11**, 175 (2019).
55. P. Krashia, E. Spoleti, M. D'Amelio, The VTA dopaminergic system as diagnostic and therapeutical target for Alzheimer's disease. *Frontiers in Psychiatry* **13**, 1039725 (2022).

56. C. Sun, W. N. Yang, J. Martin, S. Tonegawa, Hippocampal neurons represent events as transferable units of experience. *Nature Neuroscience* **23**, 651-U117 (2020).
57. H. Eichenbaum, Time cells in the hippocampus: a new dimension for mapping memories. *Nat Rev Neurosci* **15**, 732-744 (2014).
58. J. L. Gauthier, D. W. Tank, A Dedicated Population for Reward Coding in the Hippocampus. *Neuron* **99**, 179-193 e177 (2018).
59. J. Catanese, A. Viggiano, E. Cerasti, M. B. Zugaro, S. I. Wiener, Retrospectively and Prospectively Modulated Hippocampal Place Responses Are Differentially Distributed along a Common Path in a Continuous T-Maze. *The Journal of Neuroscience* **34**, 13163-13169 (2014).
60. M. Arnold, K. Nho, A. Kueider-Paisley, T. Massaro, K. Huynh, B. Brauner, S. MahmoudianDehkordi, G. Louie, M. A. Moseley, J. W. Thompson, Sex and APOE ε4 genotype modify the Alzheimer's disease serum metabolome. *Nat. Commun.* **11**, 1148 (2020).
61. D. Sohn, K. Shpanskaya, J. E. Lucas, J. R. Petrella, A. J. Saykin, R. E. Tanzi, N. F. Samatova, P. M. Doraiswamy, Sex differences in cognitive decline in subjects with high likelihood of mild cognitive impairment due to Alzheimer's disease. *Scientific reports* **8**, 7490 (2018).
62. C. H. Poon, S. T. N. Wong, J. Roy, Y. Wang, H. W. H. Chan, H. Steinbusch, A. Blokland, Y. Temel, L. Aquili, L. W. Lim, Sex differences between neuronal loss and the early onset of amyloid deposits and behavioral consequences in 5xFAD transgenic mouse as a model for Alzheimer's disease. *Cells* **12**, 780 (2023).
63. K. R. Sadleir, W. A. Eimer, S. L. Cole, R. Vassar, Aβ reduction in BACE1 heterozygous null 5XFAD mice is associated with transgenic APP level. *Molecular neurodegeneration* **10**, 1-16 (2015).
64. T. P. O'Leary, R. E. Brown, Visuo-spatial learning and memory impairments in the 5xFAD mouse model of Alzheimer's disease: Effects of age, sex, albinism, and motor impairments. *Genes, Brain and Behavior* **21**, e12794 (2022).
65. E. Popugaeva, E. Pchitskaya, I. Bezprozvanny, Dysregulation of intracellular calcium signaling in Alzheimer's disease. *Antioxidants & redox signaling* **29**, 1176-1188 (2018).
66. D. A. Dombeck, C. D. Harvey, L. Tian, L. L. Looger, D. W. Tank, Functional imaging of hippocampal place cells at cellular resolution during virtual navigation. *Nat Neurosci* **13**, 1433-1440 (2010).
67. A. Giovannucci, J. Friedrich, P. Gunn, J. Kalfon, B. L. Brown, S. A. Koay, J. Taxidis, F. Najafi, J. L. Gauthier, P. Zhou, CaImAn an open source tool for scalable calcium imaging data analysis. *Elife* **8**, e38173 (2019).
68. W. Skaggs, B. Mcnaughton, K. Gothard, An information-theoretic approach to deciphering the hippocampal code. *Advances in neural information processing systems* **5**, (1992).